



Prognostic value of whole-body dynamic ^{18}F -FDG PET/CT Patlak in diffuse large B-cell lymphoma

Jiankang Yin^a, Hui Wang^b, Gan Zhu^b, Ni Chen^a, Muhammad Imran Khan^{c,d,e,*}, Ye Zhao^{a,**}

^a School of Basic Medical Sciences, Anhui Medical University, Hefei, PR China

^b Department of Nuclear Medicine, The First Affiliated Hospital of Anhui Medical University, Hefei, 230032, Anhui, PR China

^c School of Life Sciences and Medicine, University of Science and Technology of China, Hefei, 230026, Anhui, PR China

^d Department of Pathology, District Headquarters Hospital, Jhang, 35200, Punjab Province, Pakistan

^e Hefei National Lab for Physical Sciences at Microscale and the Center for Biomedical Engineering, University of Science and Technology of China, Hefei, 230026, Anhui, PR China

ARTICLE INFO

Keywords:

Whole-body dynamic PET/CT
Patlak
Diffuse large B-Cell lymphoma
 ^{18}F - fluorodeoxyglucose

ABSTRACT

Objective: This study aims to investigate the significance of interim whole-body dynamic ^{18}F -fluorodeoxyglucose positron emission tomography/computed tomography (^{18}F -FDG PET/CT) Patlak parameters for predicting the prognosis of patients with diffuse large B-cell lymphoma. To estimate the predictive value of the whole-body dynamic ^{18}F -FDG PET/CT Patlak parameter for 2-year progression-free survival (PFS) and 2-year overall survival (OS).

Methods: This study reports the findings of 67 patients with diffuse large B-cell lymphoma (DLBCL). These patients underwent interim whole-body dynamic ^{18}F -FDG PET/CT scans from June 2021 to January 2023 at the Department of Nuclear Medicine, First Affiliated Hospital of Anhui Medical University. The predictive values of maximum standard uptake value (SUV_{max}), maximum of net glucose uptake rate ($\text{K}_{\text{i,max}}$) and the predictive model combining $\text{K}_{\text{i,max}}$ and interim treatment response on the prognosis of patients was analyzed using receiver operating characteristic (ROC) curves. Kaplan-Meier survival curves and log-rank tests were used for survival analysis. Univariate and multivariate analyses were performed to screen for independent prognostic risk factors.

Results: After a median follow-up of 18 months, 21 patients (31.3%) experienced disease recurrence or death. The cut-off values for the SUV_{max} and the $\text{K}_{\text{i,max}}$ were 6.1 and $0.13 \mu\text{mol min}^{-1} \cdot \text{ml}^{-1}$, respectively. Ann Arbor stage, IPI, SUV_{max} , $\text{K}_{\text{i,max}}$ and interim treatment response were associated with PFS and OS in the univariate analysis. However, only $\text{K}_{\text{i,max}}$ and interim treatment response were independent influences on PFS and OS in multivariate analysis.

Conclusion: Interim whole-body dynamic ^{18}F -FDG PET/CT Patlak imaging has significant prognostic value in patients with DLBCL. Among them, the interim dynamic parameter $\text{K}_{\text{i,max}}$ showed the best predictive value for prognosis compared with the interim SUV_{max} and interim treatment response. The predictive model established by $\text{K}_{\text{i,max}}$ and the interim treatment response allowed for the accurate stratification of the prognostic risk of DLBCL.

* Corresponding author. School of Life Sciences and Medicine, University of Science and Technology of China, Hefei, 230036, Anhui, PR China.

** Corresponding author. School of Basic Medical Sciences, Anhui Medical University, Hefei, PR China

E-mail addresses: imranalmani@mail.ustc.edu.cn (M.I. Khan), zhaoye@ahmu.edu.cn (Y. Zhao).

<https://doi.org/10.1016/j.heliyon.2023.e19749>

Received 27 May 2023; Received in revised form 23 August 2023; Accepted 31 August 2023

Available online 1 September 2023

2405-8440/© 2023 The Authors. Published by Elsevier Ltd. This is an open access article under the CC BY-NC-ND license (<http://creativecommons.org/licenses/by-nc-nd/4.0/>).

1. Introduction

Diffuse large B-cell lymphoma (DLBCL) is a subtype of non-Hodgkin's lymphoma [1,2]. Chemotherapy, the most widely used clinical treatment for DLBCL, can cure more than half of the patients, but 30–40% of them experience relapse or death after cure. It is widely recognized that the high recurrence rate of DLBCL is closely related to its high heterogeneity. Furthermore, the prognosis of different patients varies greatly due to genetic and immunophenotypic factors [2–4]. Therefore, it is important to accurately predict patient prognosis during the treatment phase to adjust treatment strategies and improve survival rates.

^{18}F -fluorodeoxyglucose positron emission tomography/computed tomography (^{18}F -FDG PET/CT) imaging is currently the most widely recognized clinical tool for assessing tumor status and guiding the personalized treatment of DLBCL [5]. However, because conventional ^{18}F -FDG PET/CT metabolic parameters only reflect the total uptake value of the tracer at the tumor site and no information on net tumor uptake can be obtained, their application for the of DLBCL patient's prognosis lacks efficacy and is greatly limited [6]. As a glucose analog, fluorodeoxyglucose (FDG) is taken up by cells using glucose at high levels. After FDG phosphorylation, it produces ^{18}F -FDG-6-phosphate, which is then almost completely captured by the radiotracer. The atrial model of FDG was established based on the above process (Fig. 1), where K1 reflects the transport rate of FDG from blood vessels to tissue cells, K2 represents the transport rate of FDG from cells to blood vessels, and K3 represents the rate of intracellular FDG phosphorylation to FDG-6-P (^{18}F -FDG-6-phosphate) [7,8]. Whole-body dynamic ^{18}F -FDG PET/CT Patlak imaging uses the above process to apply the FDG two-compartment kinetic model to assess the K1, K2, and K3 rate coefficients and calculate the Ki values. Whole-body dynamic ^{18}F -FDG PET/CT Patlak imaging can obtain multiple images of pharmacokinetic parameters, such as MR_{FDG} (metabolic rate of FDG) images. These reflect dephosphorylated FDG by cells and DV_{FDG} (distribution volume of free FDG) images of the volumetric distribution of free FDG. Among them, maximum of net glucose uptake rate (Ki_{max}) obtained from MR_{FDG} images is a popular parameter for current research because of its ability to reflect the maximum net uptake of FDG by tumor tissues [9,10]. The present study focuses on the prognostic predictive value of the whole-body dynamic ^{18}F -FDG PET/CT Patlak parameter Ki_{max} in patients with DLBCL.

2. Materials and methods

2.1. Subjects

Between June 2021 and January 2023, 121 patients with DLBCL were admitted to the First Affiliated Hospital of Anhui Medical University, Hefei. Of them, 54 patients were excluded due to falling in exclusion criteria, such as 16 patients did not undergo baseline PET/CT, 11 patients received other therapies before whole-body dynamic PET/CT, 13 patients dropped out during the course of treatment or follow-up, or had incomplete clinical records ($n = 14$). Finally, a total of 67 patients were included in this study. The inclusion criteria were as follows: (a) DLBCL confirmed by pathological biopsy, (b) 2–4 cycles of rituximab, cyclophosphamide, doxorubicin, vincristine, and prednisone (R-CHOP) like chemotherapy after the baseline scan, (c) patients who could cooperate with the examination, (d) patients who underwent baseline and end PET/CT at the said hospital, and (e) patients with complete clinical data. The exclusion criteria were as follows: (a) suffering from other malignant lesions at the same time; (b) complete surgical resection of the lesion; (c) radiation therapy during treatment; (d) missing clinical data.

2.2. ^{18}F -FDG PET/CT Patlak

Patients with newly diagnosed DLBCL underwent an interim dynamic ^{18}F -FDG PET/CT Patlak scan after 2–4 cycles of chemotherapy. A Siemens Biograph Vision PET/CT machine was used, and ^{18}F -FDG was purchased from Nanjing Jiangyuan Dike Positron Research and Development Company. Patients were instructed to fast for at least 8 h prior to the scan, with an optimal blood glucose level of less than 8 mmol/L. The study participants and their families were informed of the examination procedure, purpose, and advantages.

Conventional whole-body dynamic PET/CT requires a continuous PET scan of 60 min and a long examination time. This leads to great limitation in its clinical application. To cope with the shortcomings of conventional whole-body dynamic PET scans, which take a long time, a 15-min multichannel continuous-bed-motion (CBM) PET acquisition sequence was used in this study. In addition, a

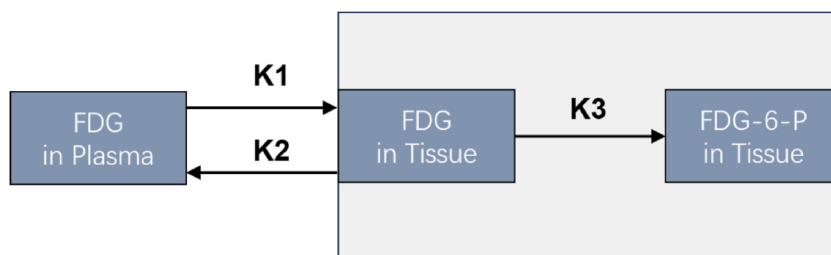


Fig. 1. FDG atrial model characterization process. FDG = fluorodeoxyglucose; K1= FDG flow rates for the total metabolic fractions; K2= FDG flow rates for the free (reversible) fractions; K3 = the FDG flow rates for the net uptake (irreversible) fractions; FDG-6-P= FDG-6-phosphate.

population-based input function commonly referred to as the Feng Input Function was used. This method greatly reduces the examination time compared with conventional whole-body dynamic PET/CT and increases the possibility of the clinical application of whole-body dynamic PET/CT. In addition, it has been demonstrated that the data from 15-min CBM acquisition with population-based input functions are not significantly different from those obtained using conventional whole-body dynamic PET/CT acquisition [11].

First, the patient was scanned using spiral CT (tube current 43 mA/s, tube voltage 100 KV, layer thickness, 1.0 mm). Thereafter, patients were given an intravenous injection of (3.7 ± 1.05) MBq/kg ^{18}F -FDG injection tracer along with PET cardiac single-bed list-mode acquisition. Finally, dynamic PET acquisition consisted of a 15-min serial dynamic acquisition, starting 45 min after injection, scanning from the superior orbital rim to the superior femur. The proposed full-body scan protocol included three full-body scans of the entire body.

The region of interest (ROI) was drawn in the patient’s aorta using a $10 \times 10 \times 2$ mm cylinder placed approximately 10 cm below the aortic arch and used as a population-based input function. The hybrid input function was obtained by fitting an exponential model to the input functions obtained from the patient’s thoracic aortic contour and three full-body scans after 45 min. A hybrid input function was used to derive the whole-body Patlak images. Moreover, MR_{FDG} images showing the net uptake information of the lesion by the tracer, and standard uptake value (SUV) images showing the total uptake information of the lesion were acquired simultaneously after Patlak reconstruction. All PET/CT images were obtained independently by two diagnostically experienced nuclear medicine physicians, with differing opinions discussed and decided upon by specialists. The ROI technique was applied to measure the maximum standard uptake value (SUV_{max}), outline the highest metabolic site on PET/CT SUV images, and outline the same location on MR_{FDG} images as on SUV images. This allowed us to obtain the metabolic parameter maximum net flux rate ($\text{K}_{\text{i,max}}$) for the same site in patients after 2–4 cycles of chemotherapy. The patients were divided into complete remission (CR) and non-complete remission (n-CR) groups according to the Lugano [12] efficacy evaluation criteria for interim outcomes.

2.3. Statistical analysis

Patients were followed-up for no less than 8 months from the time of diagnosis, by telephone or on an outpatient basis. The progression-free survival (PFS) was defined as the time from diagnosis to progression or death from any cause. Overall survival (OS) was defined as the time from diagnosis to death from any cause. Patients who were still alive were censored at the date of last contact, or last follow-up.

All statistical analyses were performed by SPSS 25.0 (IBM, Armonk, NY, USA), GraphPad Prism (version 8.3.0), and R software (version 4.2.0). Receiver operating characteristic (ROC) curves were used to analyze the efficacy of SUV_{max} , $\text{K}_{\text{i,max}}$ and the combined predictive model of $\text{K}_{\text{i,max}}$ and interim treatment response for prognostic prediction. The correlation between clinical characteristics, each metabolic parameter, and prognosis was analyzed using the chi-square test. $P < 0.05$ was considered statistically significant at $P < 0.05$. Survival analysis was performed using the Kaplan-Meier (K-M) method, and differences between groups were tested using the

Table 1
Relationship between clinical features and prognosis.

| Covariate | Total (%) | 2-year PFS | χ^2 | P-value | 2-year OS | χ^2 | P-value |
|-----------------|-----------|------------|----------|---------|-----------|----------|-----------|
| Age, years | | | 0.295 | 0.587 | | 0.087 | 0.768 |
| ≥ 54 | 35(52.2) | 23 | | | 24 | | |
| < 54 | 32(47.8) | 23 | | | 23 | | |
| Gender | | | 0.046 | 0.831 | | 0.315 | 0.575 |
| Male | 30(44.8) | 21 | | | 20 | | |
| Female | 37(55.2) | 25 | | | 27 | | |
| Ann Arbor stage | | | 8.688 | 0.003 | | 14.050 | < 0.001 |
| I/II | 48(71.6) | 38 | | | 40 | | |
| III/IV | 19(28.4) | 8 | | | 7 | | |
| BMI | | | 0.295 | 0.587 | | 1.861 | 0.173 |
| ≥ 22.8 | 35(52.2) | 23 | | | 22 | | |
| < 22.8 | 32(47.8) | 23 | | | 25 | | |
| IPI | | | 11.783 | 0.001 | | 13.216 | < 0.001 |
| > 2 | 17(25.4) | 6 | | | 6 | | |
| ≤ 2 | 50(74.6) | 40 | | | 41 | | |
| LDH | | | 0.648 | 0.421 | | 0.993 | 0.319 |
| Normal | 46(68.7) | 33 | | | 34 | | |
| Abnormal | 21(31.3) | 13 | | | 13 | | |
| $\beta 2$ -M | | | 1.959 | 0.162 | | 4.910 | 0.027 |
| Normal | 34(50.7) | 26 | | | 28 | | |
| Abnormal | 33(49.3) | 20 | | | 19 | | |
| Bcl-2 | | | 1.234 | 0.267 | | 3.882 | 0.049 |
| + | 38(56.7) | 24 | | | 23 | | |
| – | 29(43.3) | 22 | | | 24 | | |
| Bcl-6 | | | 1.410 | 0.235 | | 3.886 | 0.049 |
| + | 28(71.8) | 17 | | | 16 | | |
| – | 39(28.2) | 29 | | | 31 | | |

BMI= Body Mass Index; IPI = international prognostic index; 2-year PFS = 2-year progression-free survival; 2-year OS = 2-year overall survival.

log-rank test. Univariate and multivariate regression analyses were performed using the COX risk model.

3. Results

3.1. Relationship between clinical features and prognosis

The enrolled patients included 30 men and 37 women, aged 54 years (18–75), with a body mass index (BMI) of 22.84 (16.94–32.18). The median follow-up time was 18 months (8–24), 2-year PFS was 68.7% (46/67) and the 2-year OS was 70.1% (47/67). Ann Arbor stage: 48 cases were in the limited stage (stage I/II) and 19 cases were in the progressive stage (stage III/IV). The 2-year PFS was associated with Ann Arbor stage and the international prognostic index (IPI). We also observed that the 2-year OS was associated with Ann Arbor stage, IPI, β 2-M, BcL-2, and BcL-6 simultaneously (Table 1).

3.2. ROC analysis of prognosis on DLBCL

The optimal $K_{i_{max}}$ value obtained from the ROC curves was $0.13 \mu\text{mol min}^{-1}\cdot\text{ml}^{-1}$, corresponding to an area under curve (AUC) of 0.798 (Fig. 2), sensitivity of 0.891, negative predictive value (NPV) of 76.2%, and positive predictive value (PPV) of 89.1%. The optimal cutoff value of SUV_{max} obtained from the ROC curve was 6.1, corresponding to an AUC of 0.794, sensitivity of 0.714, specificity of 0.826, NPV of 59.3%, and PPV of 87.5%. The interim treatment response had a sensitivity, specificity, NPV, and PPV of 76.2%, 87.0%, 72.7%, and 88.9%, respectively (Table 2).

Of the five patients with an interim n-CR treatment response, who relapsed after follow-up, four were positive for interim $K_{i_{max}}$ (Fig. 3 (a-d)). $K_{i_{max}}$ showed better prognostic power than interim SUV_{max} and interim treatment response in patients with DLBCL in terms of AUC, positive predictive value, or negative predictive value.

3.3. Relationship between PET/CT parameters and prognosis

The 2-year PFS of patients in the $K_{i_{max}} < 0.11 \mu\text{mol min}^{-1}\cdot\text{ml}^{-1}$ group, $\text{SUV}_{max} < 6.1$, and CR groups were significantly better than those in the $K_{i_{max}} \geq 0.11 \mu\text{mol min}^{-1}\cdot\text{ml}^{-1}$ group, $\text{SUV}_{max} \geq 6.1$ group, and n-CR groups, respectively ($\chi^2 = 28.588$, $P < 0.001$; $\chi^2 = 18.675$, $P < 0.001$; and $\chi^2 = 26.069$, $P < 0.001$). Similarly, the 2-year OS of patients in the $K_{i_{max}} < 0.11 \mu\text{mol min}^{-1}\cdot\text{ml}^{-1}$ group, $\text{SUV}_{max} < 6.1$, and CR groups were significantly better than those in the $K_{i_{max}} \geq 0.11 \mu\text{mol min}^{-1}\cdot\text{ml}^{-1}$ group, $\text{SUV}_{max} \geq 6.1$ group and n-CR groups, respectively ($\chi^2 = 25.251$, $P < 0.001$; $\chi^2 = 20.920$, $P < 0.001$; and $\chi^2 = 22.983$, $P < 0.001$, Table 3).

3.4. Univariate and multivariate analysis of 2-year PFS and OS on DLBCL

Ann Arbor staging, IPI, SUV_{max} , $K_{i_{max}}$ and interim treatment response all exhibited significant predictive values for PFS in the univariate Cox analysis. (HR = 2.974, 95% CI 1.2641–7.013, $P = 0.013$, and HR = 3.404, 95% CI 1.444–8.028, $P = 0.005$, and HR = 7.251, 95% CI 2.786–18.875, $P < 0.001$, and HR = 9.465, 95% CI 3.843–26.059, $P < 0.001$, and HR = 10.388, 95% CI

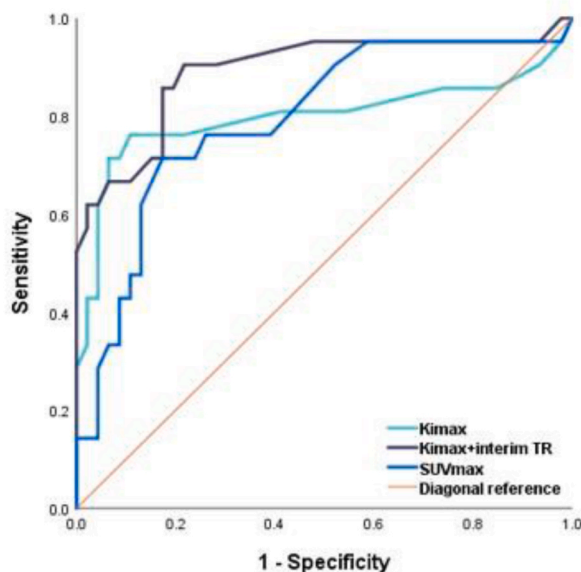


Fig. 2. Receiver operator characteristics (ROC) analysis. Interim TR = interim treatment response; $K_{i_{max}}$ = the maximum of net flux rate (the maximum value of Patlak slope); SUV_{max} = the maximum of standard uptake value.

Table 2
Sensitivity, Specificity, PPV and NPV values.

| | Ki _{max} (%) | SUV _{max} (%) | Interim treatment response (%) | Ki _{max} & Interim treatment response (%) |
|-------------|-----------------------|------------------------|--------------------------------|--|
| Sensitivity | 76.2 | 71.4 | 76.2 | 61.9 |
| Specificity | 89.1 | 82.6 | 87.0 | 76.1 |
| PPV | 76.2 | 65.2 | 72.7 | 92.9 |
| NPV | 89.1 | 86.4 | 88.9 | 97.2 |

Ki_{max} = the maximum of net glucose uptake rate (the maximum value of Patlak slope); SUV_{max} = the maximum of standard uptake value; PPV = positive predictive value; NPV = negative predictive value.

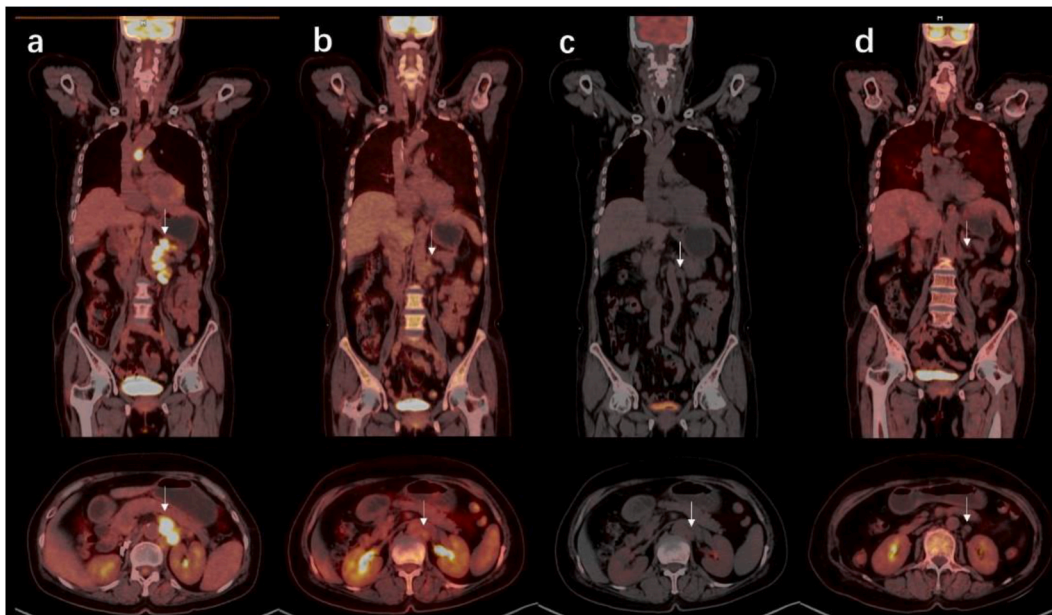


Fig. 3. A 64-year-old female patient with DLBCL who initially showed n-CR in interim treatment response but had an end-PET suggestive of CR is still alive and free of disease at the 24-month follow-up. The patient had multiple enlarged lymph nodes in the retroperitoneum as seen in the baseline ¹⁸F-FDG PET/CT SUV fusion image (a). After receiving 4 courses of R-CHOP treatment, the interim ¹⁸F-FDG PET/CT SUV fusion image still showed metabolized lesions at the site, indicating a non-complete response (n-CR) (b). At this time, the MR_{FDG} fusion image did not reveal any significant abnormal FDG metabolism (c). After receiving 4 more courses of chemotherapy, the end-¹⁸F-FDG PET/CT SUV fusion image suggested complete response (CR) (Deauville:2 points) (d).

Table 3
Relationship between ¹⁸F-FDG PET/CT Patlak parameters and prognosis.

| Covariate | Total (%) | 2-year PFS | χ^2 | P | 2-year OS | χ^2 | P |
|--------------------|-----------|------------|----------|--------|-----------|----------|--------|
| SUV _{max} | | | 18.675 | <0.001 | | 20.920 | <0.001 |
| ≥6.1 | 23(34.3) | 8 | | | 8 | | |
| <6.1 | 44(65.7) | 38 | | | 39 | | |
| Ki _{max} | | | 28.588 | <0.001 | | 25.251 | <0.001 |
| ≥0.13 | 21(31.3) | 5 | | | 6 | | |
| <0.13 | 46(68.7) | 41 | | | 41 | | |
| Interim TR | | | 26.069 | <0.001 | | 22.983 | <0.001 |
| CR | 45(67.2) | 40 | | | 40 | | |
| n-CR | 22(22.8) | 6 | | | 7 | | |

Interim TR = interim treatment response; Ki_{max} = the maximum of net flux rate (the maximum value of Patlak slope); SUV_{max} = the maximum of standard uptake value; 2-year PFS = 2-year progression-free survival; 2-year OS = 2-year overall survival.

3.726–28.959, $P < 0.001$, Table 4). Additionally, these five factors also exhibited significant influence on OS (HR = 4.235, 95% CI 1.722–10.417, $P = 0.002$, and HR = 4.494, 95% CI 1.817–11.100, $P = 0.001$, and HR = 6.881, 95% CI 2.496–18.970, $P < 0.001$, and HR = 9.730, 95% CI 3.444–27.485, $P < 0.001$, and HR = 7.352, 95% CI 2.665–20.281, $P < 0.001$, respectively). Owing to the strong correlation between Ann Arbor stage and IPI, only IPI was included in the multivariate COX regression analysis. Eventually, IPI, Ki_{max}, interim treatment response, and SUV_{max} were entered into the multivariate COX regression analysis, and only Ki_{max} and interim

Table 4
Univariate analysis of 2-year PFS and 2-year OS on DLBCL.

| | PFS | | | | OS | | | |
|-------------------------------------|--------|-------|--------|--------|-------|-------|--------|--------|
| | HR | 95%CI | | P | HR | 95%CI | | P |
| Age (<54 VS ≥ 54) | 1.099 | 0.462 | 2.614 | 0.831 | 1.149 | 0.475 | 2.778 | 0.758 |
| Gender (Male VS Female) | 0.937 | 0.394 | 2.226 | 0.882 | 0.523 | 0.215 | 1.273 | 0.153 |
| BMI (≥22.8 VS < 22.8) | 1.165 | 0.489 | 2.774 | 0.730 | 1.763 | 0.703 | 4.422 | 0.227 |
| Ann Arbor (I/II VS III/IV) | 2.974 | 1.261 | 7.013 | 0.013 | 4.235 | 1.722 | 10.417 | 0.002 |
| IPI (≤2 VS > 2) | 3.404 | 1.444 | 8.026 | 0.005 | 4.494 | 1.819 | 11.100 | 0.001 |
| LDH (Normal VS Abnormal) | 1.394 | 0.577 | 3.368 | 0.460 | 1.453 | 0.591 | 3.573 | 0.416 |
| β2-M (Normal VS Abnormal) | 1.558 | 0.644 | 3.768 | 0.325 | 0.960 | 0.749 | 5.129 | 0.170 |
| Bcl-2 (- VS +) | 1.896 | 0.760 | 4.731 | 0.170 | 2.760 | 0.997 | 7.645 | 0.051 |
| Bcl-6 (- VS +) | 1.491 | 0.631 | 3.523 | 0.363 | 1.491 | 0.631 | 3.523 | 0.363 |
| SUV _{max} (<6.1 VS ≥ 6.1) | 7.251 | 2.786 | 18.875 | <0.001 | 6.881 | 2.496 | 18.970 | <0.001 |
| Ki _{max} (<0.13 VS ≥ 0.13) | 9.465 | 3.843 | 26.059 | <0.001 | 9.730 | 3.444 | 27.485 | <0.001 |
| Interim TR (CR VS n-CR) | 10.388 | 3.726 | 28.959 | <0.001 | 7.352 | 2.665 | 20.281 | <0.001 |

BMI= Body Mass Index; IPI = international prognostic index; Interim TR = interim treatment response; Ki_{max} = the maximum of net flux rate (the maximum value of Patlak slope); SUV_{max} = the maximum of standard uptake value; PFS = 2-year progression-free survival; OS = 2-year overall survival.

treatment response independently showed predictive value in patients ($P = 0.020$ and $P = 0.026$ Table 5, Fig. 4).

3.5. Kaplan-Meier survival curve analysis

The results of DLBCLs' 2-year PFS for the semiquantitative and quantitative analysis using Ki_{max} and interim treatment response were as follows: 89.1% for patients with Ki_{max} < 0.13 μmol min⁻¹.ml⁻¹. In contrast to 23.8% for patients with Ki_{max} ≥ 0.13 μmol min⁻¹.ml⁻¹ ($P < 0.001$, Fig. 5(a)); 88.9% for patients with CR contrast to 27.3% for patients with n-CR ($P < 0.001$, Fig. 5(b)). Further, the results of DLBCLs' 2-year OS for the semiquantitative and quantitative analysis using Ki_{max} and interim treatment response were as follows: 89.1% for patients with Ki_{max} < 0.13 μmol min⁻¹.ml⁻¹ in contrast to 28.6% for patients with Ki_{max} ≥ 0.13 μmol min⁻¹.ml⁻¹ ($P < 0.001$, Fig. 5(c)); 88.9% for patients with CR contrast to 31.8% for patients with n-CR ($P = 0.0013$, Fig. 5(d)).

3.6. Predictive model

ROC curves were plotted for the combined predictive model of Ki_{max} and interim treatment response, and the area under the curve was 0.891. In addition, the predictive model predicted a 92.9% and 97.2% for the PPV and NPV of PFS, respectively, both of which were significantly better than their respective values. Therefore, we tentatively consider that combining the two can significantly improve the prognostic predictive efficacy.

After that, combining the Ki_{max} and interim treatment response to construct a predictive model, patients were divided into three risk groups: high risk: Ki_{max} ≥ 0.13 + n-CR group, low risk: Ki_{max} < 0.13 + CR group, and medium risk: Ki_{max} ≥ 0.13 + CR group or Ki_{max} < 0.13 + n-CR group. In addition, the KM survival curve analysis of the predictive model showed that patients in the high-risk group had the worst prognosis (PFS:7.1%, $P < 0.001$; OS:7.1%, $P < 0.001$) and those in the medium-risk group had a moderate prognosis (PFS:58.8%, $P < 0.001$; OS:76.5%, $P < 0.001$). Finally, those in the low-risk group had the best prognosis (PFS:97.2%, $P < 0.001$; OS:91.7%, $P < 0.001$; Fig. 6(a) and b).

4. Discussion

It is extremely important to explore reliable parameters to identify patients with DLBCL, with a poor prognosis. Currently, the IPI is commonly used clinically to predict prognosis and in risk stratification [13]. Several authors [14,15] have analyzed the impact of IPI on prognosis and found that IPI is an independent prognostic factor in patients with DLBCL. In contrast to their results, the present study found that IPI was only an influential factor in patient prognosis and not an independent influence, which is the same as the

Table 5
Multivariate analysis of 2-year PFS and OS on DLBCL.

| | PFS | | | | OS | | | |
|-------------------------------------|-------|-------|--------|-------|-------|-------|--------|-------|
| | HR | 95%CI | | P | HR | 95%CI | | P |
| IPI (≤2 VS > 2) | 1.400 | 0.560 | 3.498 | 0.471 | 2.147 | 0.739 | 6.236 | 0.160 |
| SUV _{max} (<6.1 VS ≥ 6.1) | 0.349 | 0.051 | 2.395 | 0.284 | 0.611 | 0.100 | 3.734 | 0.594 |
| Ki _{max} (<0.13 VS ≥ 0.13) | 6.857 | 1.487 | 31.610 | 0.014 | 5.234 | 1.293 | 21.191 | 0.020 |
| Interim TR (CR VS n-CR) | 9.494 | 1.923 | 46.871 | 0.006 | 5.871 | 1.234 | 27.932 | 0.026 |

Ki_{max} = the maximum of net flux rate (the maximum value of Patlak slope); SUV_{max} = the maximum of standard uptake value; PFS = 2-year progression-free survival; OS = 2-year overall survival.

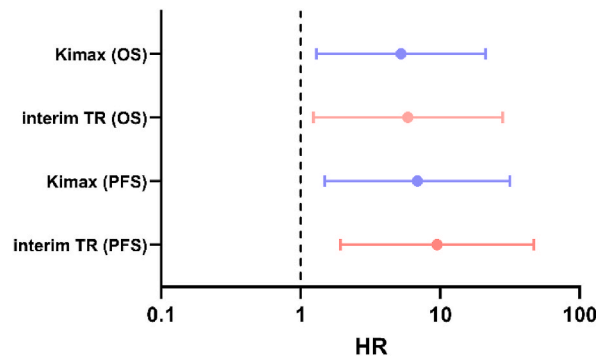


Fig. 4. Comparison of hazard ratios (positive versus negative groups) and 95% confidence intervals for various interpretation methods, including $K_{i_{max}}$ and interim treatment response. $K_{i_{max}}$ = the maximum of net flux rate (the maximum value of Patlak slope); interim TR = interim treatment response; PFS = 2-year progression-free survival; OS = 2-year overall survival.

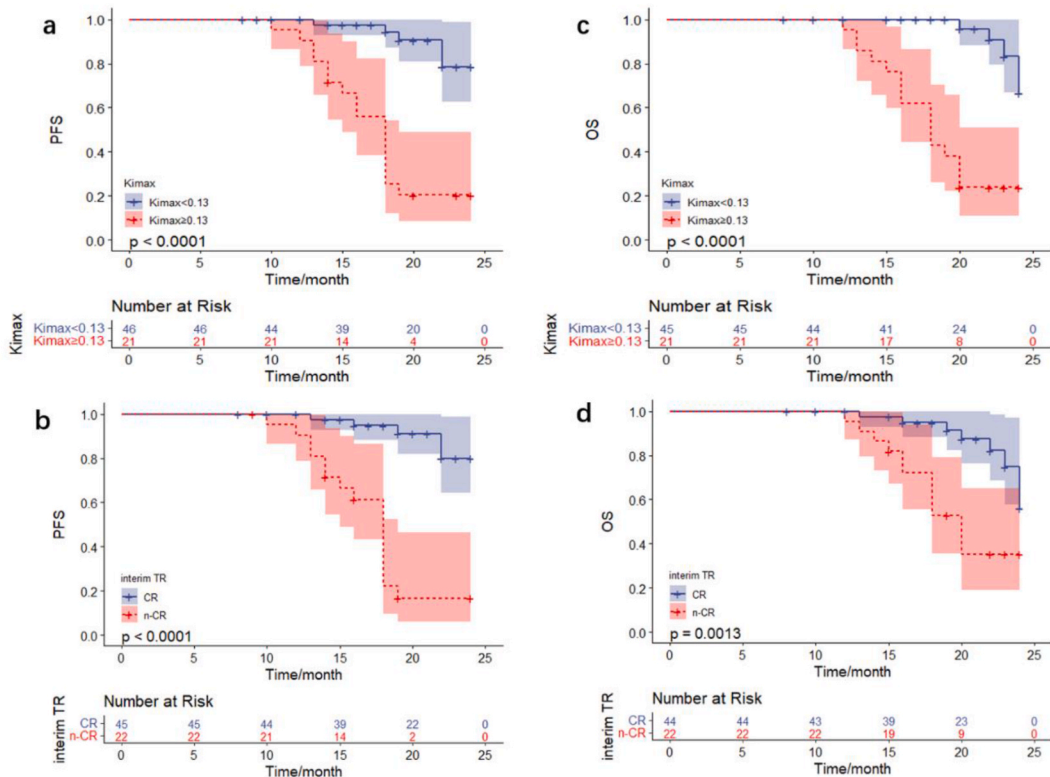


Fig. 5. Kaplan-Meier curves of 2-year progression-free survival and 2-year overall survival of diffuse large B-cell lymphoma patients according to $K_{i_{max}}$ (cutoff, $0.13 \mu\text{mol min}^{-1}\cdot\text{ml}^{-1}$, a and c) and interim treatment response (b and d). $K_{i_{max}}$ = the maximum of net flux rate (the maximum value of Patlak slope); Interim TR = interim treatment response; CR = complete remission; n-CR = non-complete remission.

findings of Tokola et al. [16] Because of the high heterogeneity of DLBCL [17,18], individual characteristics and response to chemotherapy are considered to be the best predictors of prognosis.

Interim ^{18}F -FDG PET/CT is now commonly used for lymphoma efficacy evaluation and prognostic prediction, and is included in the “2021 CSCO lymphoma ^{18}F -FDG PET/CT guidelines”. SUV_{max} is used as a static ^{18}F -FDG PET/CT parameter to assess tumor metabolism, owing to its easy availability and reproducibility and reflects tumor burden. However, SUV_{max} is susceptible to factors such as patient blood glucose, uptake time, acquisition and reconstruction methods, equipment, and population heterogeneity [19,20]. This is especially for low-uptake lesions, where uptake values often lead to false-positive results due to high background uptake. In contrast, whole-body dynamic ^{18}F -FDG PET/CT Patlak imaging provides information on drug metabolism in vivo, over time, allowing conventional SUV, MR_{FDG} , and DV_{FDG} images to be obtained simultaneously. FDG-6-P, which is generated after phosphorylation by hexokinase from FDG injected into patients, cannot participate in glycogen synthesis or glycolysis, and is trapped in cells. The Patlak

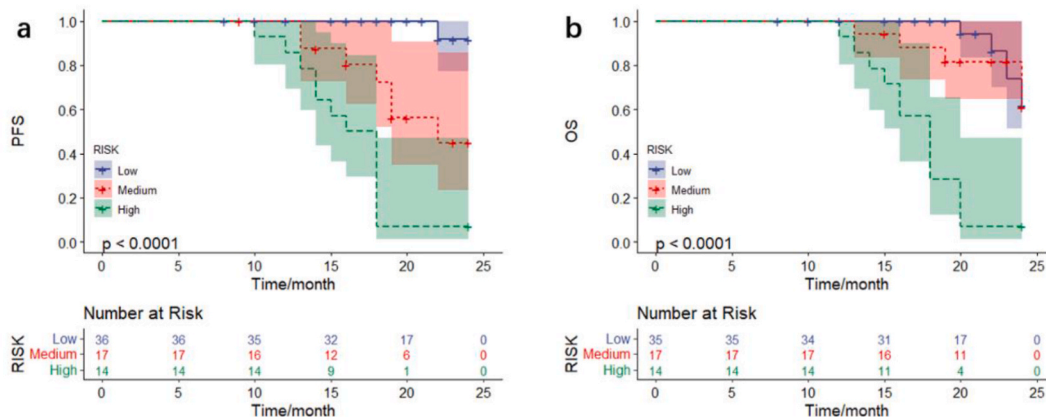


Fig. 6. 2-year progression-free survival (a) and 2-year overall survival (b) according to the predictive model. High: $Ki_{max} \geq 0.13 + n\text{-CR}$ group (high risk group); Low: $Ki_{max} < 0.13 + CR$ group (low risk group); Medium: $Ki_{max} \geq 0.13 + CR$ group or $Ki_{max} < 0.13 + n\text{-CR}$ group (medium risk group).

image processing technique quantifies the above process for whole-body dynamic ^{18}F -FDG PET/CT, which in turn fits and estimates the Patlak slope Ki and intercept Dv (distribution volume) values at each voxel of the body. $Ki = (k_1 \times k_3) / (k_2 + k_3)$, is an indication of the net rate of tracer uptake. Consequently, the advantage of whole-body dynamic ^{18}F -FDG PET/CT over conventional static ^{18}F -FDG PET/CT is the ability to accurately quantify FDG uptake at the tumor site. The feasibility of whole-body dynamic ^{18}F -FDG PET/CT has been confirmed by increases in computing power, scanning, and algorithm development. Several researchers have proposed the role of Ki [19,21,22].

In this study, Ki_{max} exhibited higher values for the AUC, sensitivity, specificity, PPV, and NPV in prognostic prediction compared to SUV_{max} . Therefore, its predictive efficacy for prognosis was significantly superior to that of SUV_{max} .

Some studies have reported that interim treatment response has an important influence on prognosis [23]. Furthermore, that the prognosis of patients without interim efficacy evaluation is generally poor. However, there is insufficient evidence for the predictive value of interim treatment response alone for prognosis. Of the Ki_{max} -positive patients, 76.2% (16/21) relapsed/died, while, 72.7% (16/22) of the interim n-CR patients relapsed/died during the follow-up period, in this study. Therefore, the ability of the interim treatment response to differentiate between high-risk patient groups needs to be improved.

Combining various parameters to predict the prognosis of patients with DLBCL is a popular research topic. Husi et al. [24] combined TARC (thymus and activation-regulated chemokine) and interim Deauville score. Eertink et al. [25] combined tumor parameters MTV (metabolic tumor volume), SUV_{peak} (peak standardized uptake value) and $D_{maxbulk}$ (the maximal distance between the largest lesion and any other lesion) and basic clinical characteristics of patients (WHO performance status and age >60 years). Cottreau et al. [26] combined MTV with D_{max} (the distance between the 2 lesions that were farthest apart). They all found that the predictive models further improved the risk stratification of DLBCL patient staging. Because only Ki_{max} and interim treatment response influence PFS and OS in patients with DLBCL, this study combined these two influencing factors to stratify the prognostic risk of patients at an early stage and provide a reference basis for patient treatment plan adjustment. The sensitivity of Ki_{max} alone in predicting PFS was 76.2%, whereas when combined with interim treatment response, the sensitivity increased to 90.5%, at which point the specificity decreased from 89.1% to 78.3% and the AUC improved.

Furthermore, OS analysis showed that 68.2% (15/22) of patients with interim n-CR died, whereas only 92.9% (13/14) of patients in the high-risk group of the predictive model died. Meanwhile, 71.4% (15/21) of the patients who were Ki_{max} -positive died during a median follow-up of 18 months. Thus, the accuracy of prognostic prediction by the interim treatment response and Ki_{max} was significantly improved by the combination of the two.

In conclusion, the interim dynamic ^{18}F -FDG PET/CT Patlak parameter, Ki_{max} , is useful in predicting the prognosis of patients with DLBCL. Moreover, the predictive model combining Ki_{max} and interim treatment response significantly enhances the predictive efficacy compared to Ki_{max} or interim treatment response alone when assessing patient prognosis. This combined model is valuable for risk stratification in DLBCL patients. However, it's worth noting that due to variations in chemotherapy cycles (ranging from 2 to 4 cycles) among patients, the small sample size, and a relatively short follow-up period, further studies are needed to comprehensively evaluate the utility of PET dynamic parameters in assessing DLBCL treatment outcomes and prognosis. Establishing a more precise mathematical assessment model is essential for a more accurate prognosis assessment in DLBCL patients..

Ethics and consent to participate

Diagnostic techniques and patient's data reported in this study has been reported in this study has been approved by the Ethical committee of Anhui Medical university and affiliated hospitals under the reference letter No: 83230050. Besides, informed consent was obtained from all patients for the publication of images and related data included in this study.

Author contribution statement

Jiankang Yin; Hui Wang; Gan Zhu: Performed the experiments; Wrote the paper.

Chen Ni: Analyzed and interpreted the data; Contributed reagents, materials, analysis tools or data.

Muhammad Imran Khan: Analyzed and interpreted the data.

Ye Zhao: Conceived and designed the experiments; Contributed reagents, materials, analysis tools or data.

Data availability statement

Data included in article/supp. material/referenced in article.

Declaration of competing interest

The authors declare that they have no known competing financial interests or personal relationships that could have appeared to influence the work reported in this paper.

References

- [1] G.W. Wright, D.W. Huang, J.D. Phelan, Z.A. Coulibaly, S. Roulland, R.M. Young, et al., A probabilistic classification tool for genetic subtypes of diffuse large B cell lymphoma with therapeutic implications, *Cancer Cell* 37 (4) (2020) 551–568.e14, <https://doi.org/10.1016/j.ccell.2020.03.015>.
- [2] Y. Liu, S.K. Barta, Diffuse large B-cell lymphoma: 2019 update on diagnosis, risk stratification, and treatment, *Am. J. Hematol.* 94 (5) (2019) 604–616, <https://doi.org/10.1002/ajh.25460>.
- [3] T.Y. Al, C. Bailly, S. Kanoun, FDG-PET/CT in lymphoma: where do we go now? *Cancers* 13 (20) (2021) <https://doi.org/10.3390/cancers13205222>.
- [4] M.I. Khan, F. Batool, R. Ali, Q.A. Zahra, W. Wang, S. Li, G. Wang, L. Liu, S.U. Khan, M. Mansoor, M. Bilal, D. Ding, A. Kazmi, F. Li, Q. Qiu, Tailoring radiotherapies and nanotechnology for targeted treatment of solid tumors, *Coordination Chemistry Reviews* 472 (2022), 214757, <https://doi.org/10.1016/j.ccr.2022.214757>.
- [5] L. Wang, L.R. Li, K.H. Young, New agents and regimens for diffuse large B cell lymphoma, *J. Hematol. Oncol.* 13 (1) (2020) 175, <https://doi.org/10.1186/s13045-020-01011-z>.
- [6] A. Rahmim, M.A. Lodge, N.A. Karakatsanis, V.Y. Panin, Y. Zhou, A. Mcmillan, et al., Dynamic whole-body PET imaging: principles, potentials and applications, *Eur. J. Nucl. Med. Mol. Imag.* 46 (2) (2019) 501–518, <https://doi.org/10.1007/s00259-018-4153-6>.
- [7] C. Sachpekidis, J.C. Hassel, A. Kopp-Schneider, U. Haberkorn, A. Dimitrakopoulou-Strauss, Quantitative dynamic (18)F-FDG PET/CT in survival prediction of metastatic melanoma under PD-1 inhibitors, *Cancers* 13 (5) (2021), <https://doi.org/10.3390/cancers13051019>.
- [8] X.L. Huang, M.I. Khan, J. Wang, R. Ali, S.W. Ali, Q.U. Zahra, A. Kazmi, A. Lolai, Y.L. Huang, A. Hussain, M. Bilal, F. Li, B. Qiu, Role of receptor tyrosine kinases mediated signal transduction pathways in tumor growth and angiogenesis-New insight and futuristic vision, *Int J Biol Macromol* 180 (2021) 739–752, <https://doi.org/10.1016/j.ijbiomac.2021.03.075>.
- [9] S. Skawran, M. Messerli, F. Kotasidis, J. Trinckauf, C. Weyermann, K. Kudura, et al., Can dynamic whole-body FDG PET imaging differentiate between malignant and inflammatory lesions? *Life* 12 (9) (2022) <https://doi.org/10.3390/life12091350>.
- [10] N. Zaker, K. Haddad, R. Faghghi, H. Arabi, H. Zaidi, Direct inference of Patlak parametric images in whole-body PET/CT imaging using convolutional neural networks, *Eur. J. Nucl. Med. Mol. Imag.* 49 (12) (2022) 4048–4063, <https://doi.org/10.1007/s00259-022-05867-w>.
- [11] D.R. Osborne, S. Acuff, Whole-body dynamic imaging with continuous bed motion PET/CT, *Nucl. Med. Commun.* 37 (4) (2016) 428–431, <https://doi.org/10.1097/MNM.0000000000000455>.
- [12] S.F. Barrington, N.G. Mikhaeel, L. Kostakoglu, M. Meignan, M. Hutchings, S.P. Mueller, et al., Role of imaging in the staging and response assessment of lymphoma: consensus of the international conference on malignant lymphomas imaging working group, *J. Clin. Oncol.* 32 (27) (2014) 3048–3058, <https://doi.org/10.1200/JCO.2013.53.5229>.
- [13] X. Zhang, L. Chen, H. Jiang, X. He, L. Feng, M. Ni, et al., A novel analytic approach for outcome prediction in diffuse large B-cell lymphoma by [(18)F]FDG PET/CT, *Eur. J. Nucl. Med. Mol. Imag.* 49 (4) (2022) 1298–1310, <https://doi.org/10.1007/s00259-021-05572-0>.
- [14] P. Decazes, S. Becker, M.N. Toledano, P. Vera, P. Desbordes, F. Jardin, et al., Tumor fragmentation estimated by volume surface ratio of tumors measured on 18F-FDG PET/CT is an independent prognostic factor of diffuse large B-cell lymphoma, *Eur. J. Nucl. Med. Mol. Imag.* 45 (10) (2018) 1672–1679, <https://doi.org/10.1007/s00259-018-4041-0>.
- [15] T.C. El-Galaly, D. Villa, M. Alzahrani, J.W. Hansen, L.H. Sehn, D. Wilson, et al., Outcome prediction by extranodal involvement, IPI, R-IPI, and NCCN-IPI in the PET/CT and rituximab era: a Danish-Canadian study of 443 patients with diffuse-large B-cell lymphoma, *Am. J. Hematol.* 90 (11) (2015) 1041–1046, <https://doi.org/10.1002/ajh.24169>.
- [16] S. Tokola, H. Kuitunen, T. Turpeenniemi-Hujanen, O. Kuitinen, Interim and end-of-treatment PET-CT suffers from high false-positive rates in DLBCL: biopsy is needed prior to treatment decisions, *Cancer Med.* 10 (9) (2021) 3035–3044, <https://doi.org/10.1002/cam4.3867>.
- [17] L. Zhu, Y. Meng, L. Guo, H. Zhao, Y. Shi, S. Li, et al., Predictive value of baseline (18)F-FDG PET/CT and interim treatment response for the prognosis of patients with diffuse large B-cell lymphoma receiving R-CHOP chemotherapy, *Oncol. Lett.* 21 (2) (2021) 132, <https://doi.org/10.3892/ol.2020.12393>.
- [18] R. Schmitz, G.W. Wright, D.W. Huang, C.A. Johnson, J.D. Phelan, J.Q. Wang, et al., Genetics and pathogenesis of diffuse large B-cell lymphoma, *N. Engl. J. Med.* 378 (15) (2018) 1396–1407, <https://doi.org/10.1056/NEJMoa1801445>.
- [19] N. Zaker, F. Kotasidis, V. Garibotto, H. Zaidi, Assessment of lesion detectability in dynamic whole-body PET imaging using compartmental and Patlak parametric mapping, *Clin. Nucl. Med.* 45 (5) (2020) e221–e231, <https://doi.org/10.1097/RLU.0000000000002954>.
- [20] C.J. Jaskowiak, J.A. Bianco, S.B. Perlman, J.P. Fine, Influence of reconstruction iterations on 18F-FDG PET/CT standardized uptake values, *J. Nucl. Med.* 46 (3) (2005) 424–428.
- [21] G. Fahrni, N.A. Karakatsanis, G. Di Domenicantonio, V. Garibotto, H. Zaidi, Does whole-body Patlak (18)F-FDG PET imaging improve lesion detectability in clinical oncology? *Eur. Radiol.* 29 (9) (2019) 4812–4821, <https://doi.org/10.1007/s00330-018-5966-1>.
- [22] A. Marin, J.T. Murchison, K.M. Skwarski, A. Tavares, A. Fletcher, W.A. Wallace, et al., Can dynamic imaging, using (18)F-FDG PET/CT and CT perfusion differentiate between benign and malignant pulmonary nodules? *Radiol. Oncol.* 55 (3) (2021) 259–267, <https://doi.org/10.2478/raon-2021-0024>.
- [23] M.N. Zeman, E.A. Akin, R.W. Merryman, H.A. Jacene, Interim FDG-PET/CT for response assessment of lymphoma, *Semin. Nucl. Med.* 53 (3) (2023) 371–388, <https://doi.org/10.1053/j.semnucmed.2022.10.004>.
- [24] K. Husi, L.I. Pinczes, Z. Fejes, B.J. Nagy, A. Illes, Z. Miltenyi, Combined prognostic role of TARC and interim (18)F-FDG PET/CT in patients with Hodgkin lymphoma-real world observational study, *Hellenic J. Nucl. Med.* 25 (2) (2022) 125–131, <https://doi.org/10.1967/s002449912471>.
- [25] J.J. Eertink, T. van de Brug, S.E. Wieggers, G. Zwezerijnen, E. Pfaehler, P.J. Lugtenburg, et al., F-FDG PET baseline radiomics features improve the prediction of treatment outcome in diffuse large B-cell lymphoma, *Eur. J. Nucl. Med. Mol. Imag.* 49 (3) (2022) 932–942, <https://doi.org/10.1007/s00259-021-05480-3>, 18.
- [26] A.S. Cottereau, C. Nioche, A.S. Dirand, J. Clerc, F. Morschhauser, O. Casasnovas, et al., (18)F-FDG PET dissemination features in diffuse large B-cell lymphoma are predictive of outcome, *J. Nucl. Med.* 61 (1) (2020) 40–45, <https://doi.org/10.2967/jnumed.119.229450>.